8.513 Lecture 14

Coherent backscattering
Weak localization
Aharonov-Bohm effect

Light diffusion; Speckle patterns;

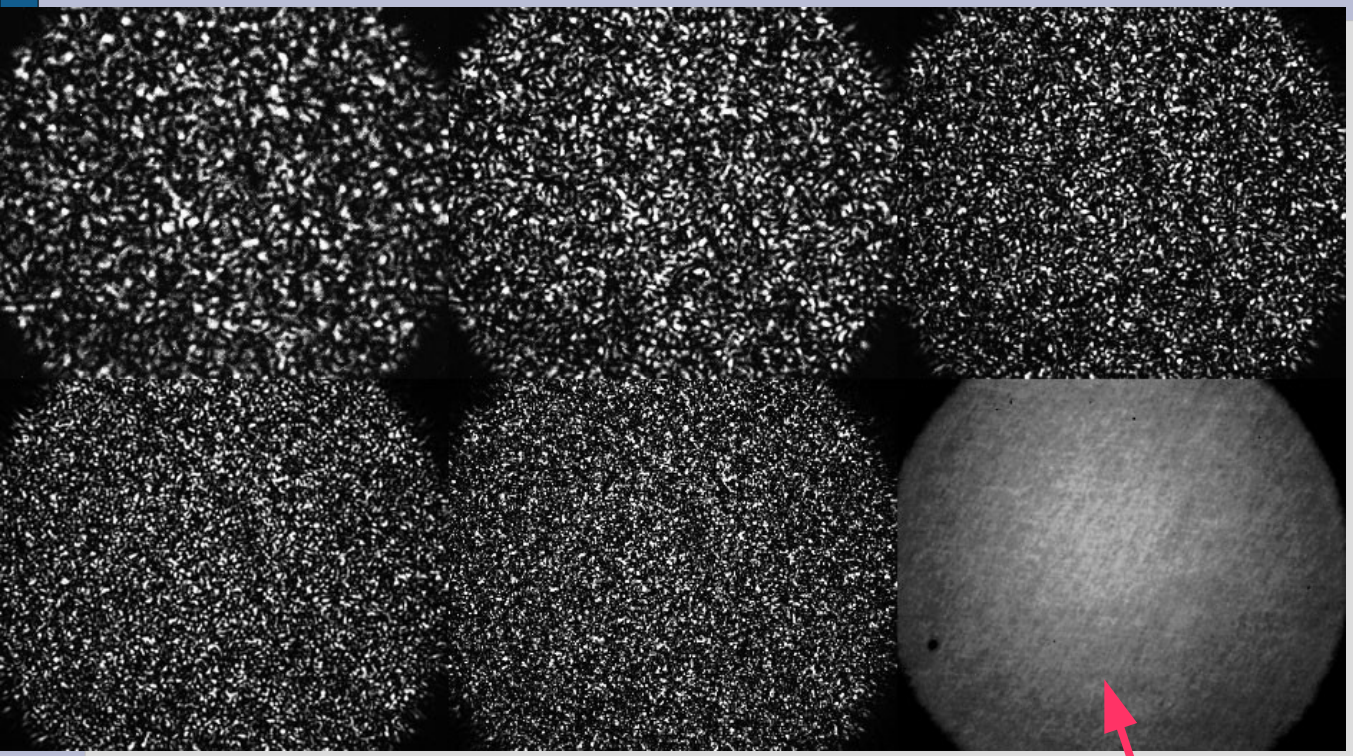

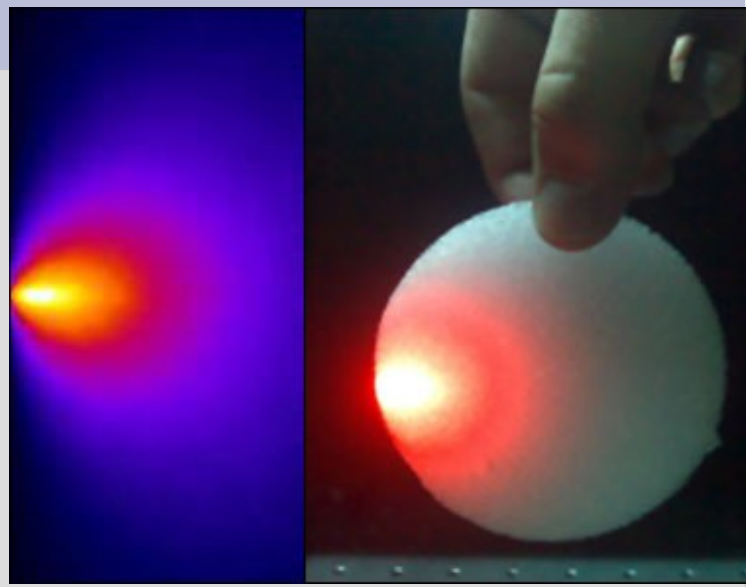

Speckles in coherent backscattering

phase-averaged

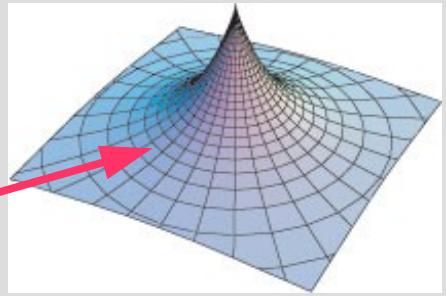

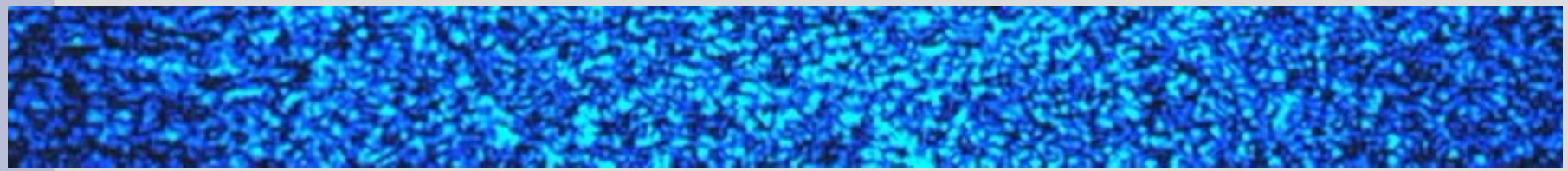

Coherent backscattering

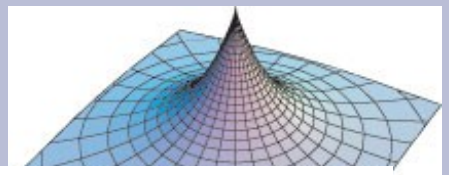

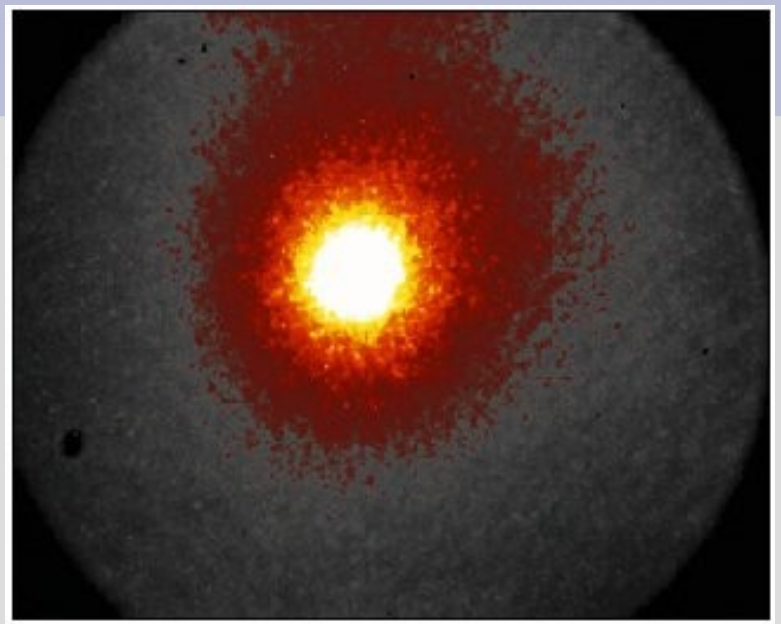

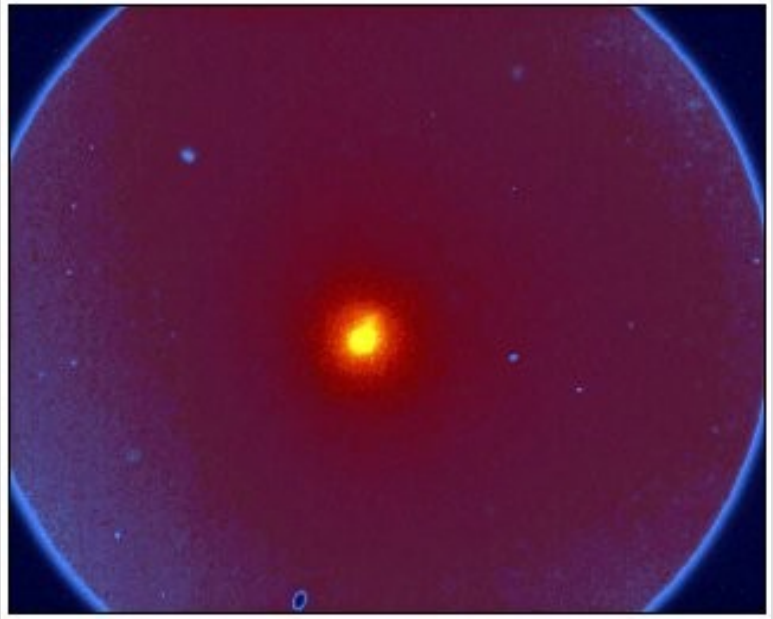

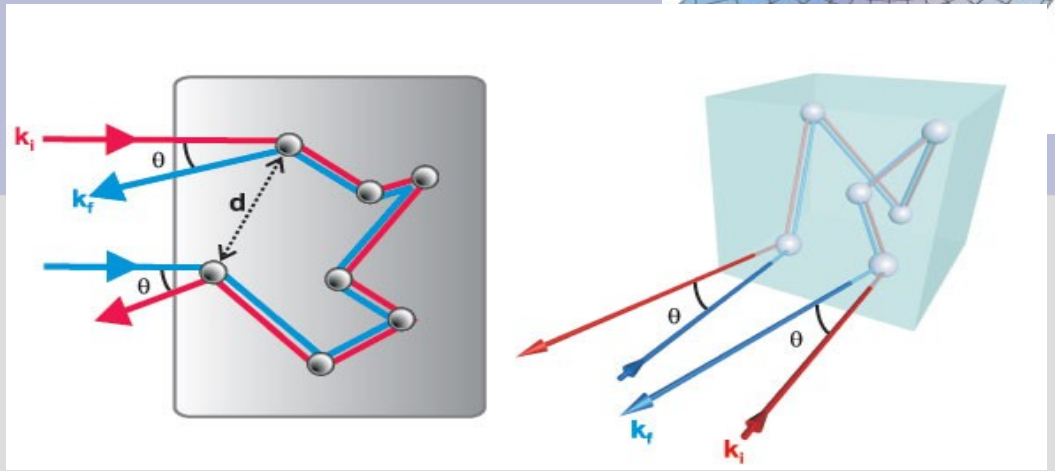

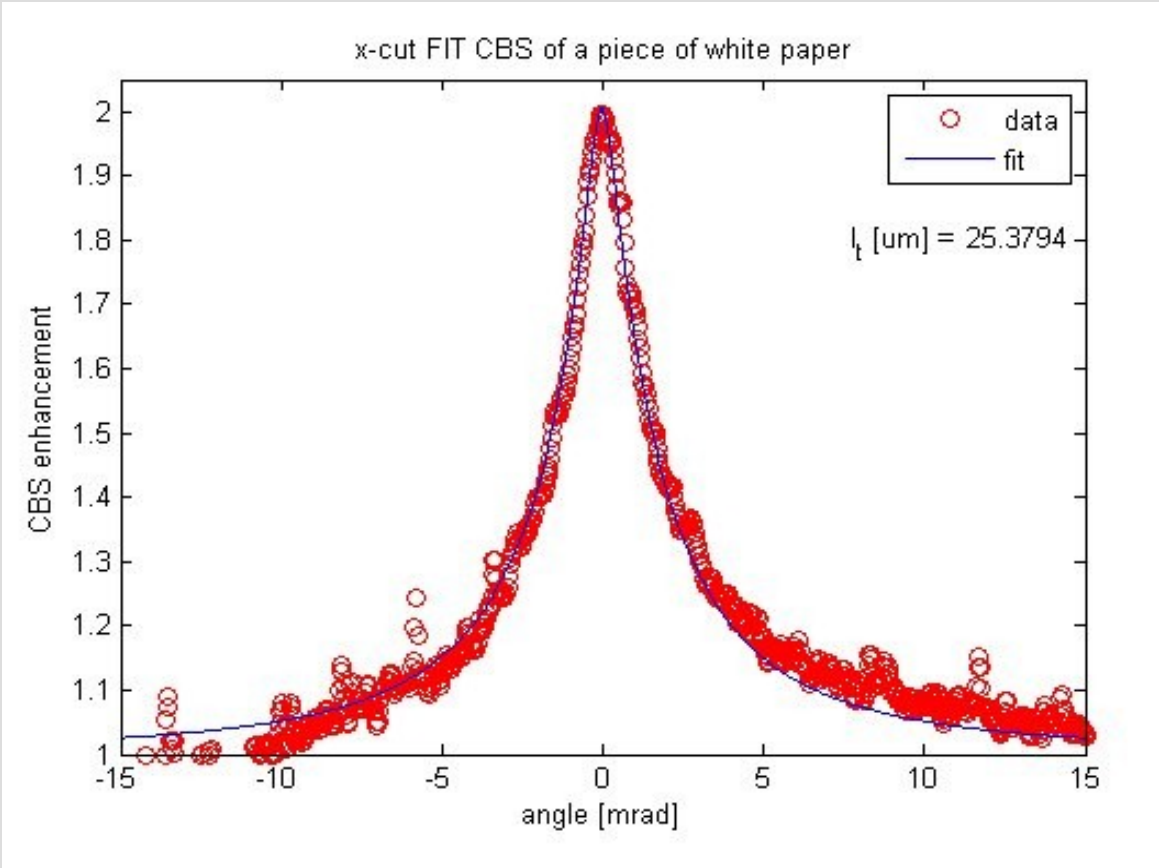

Contribution of multiple scattering processes

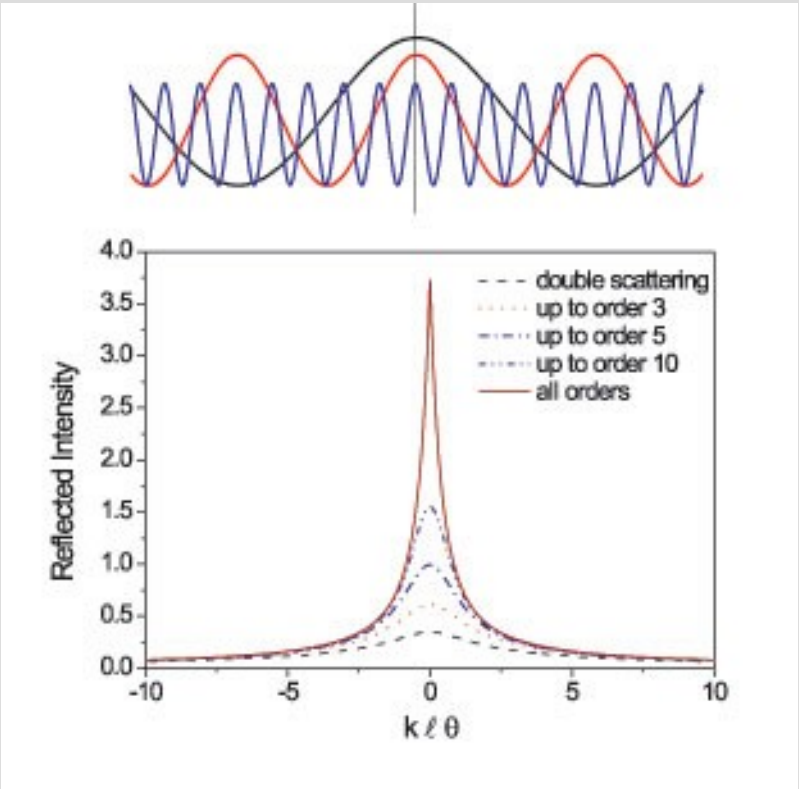

Weak localization

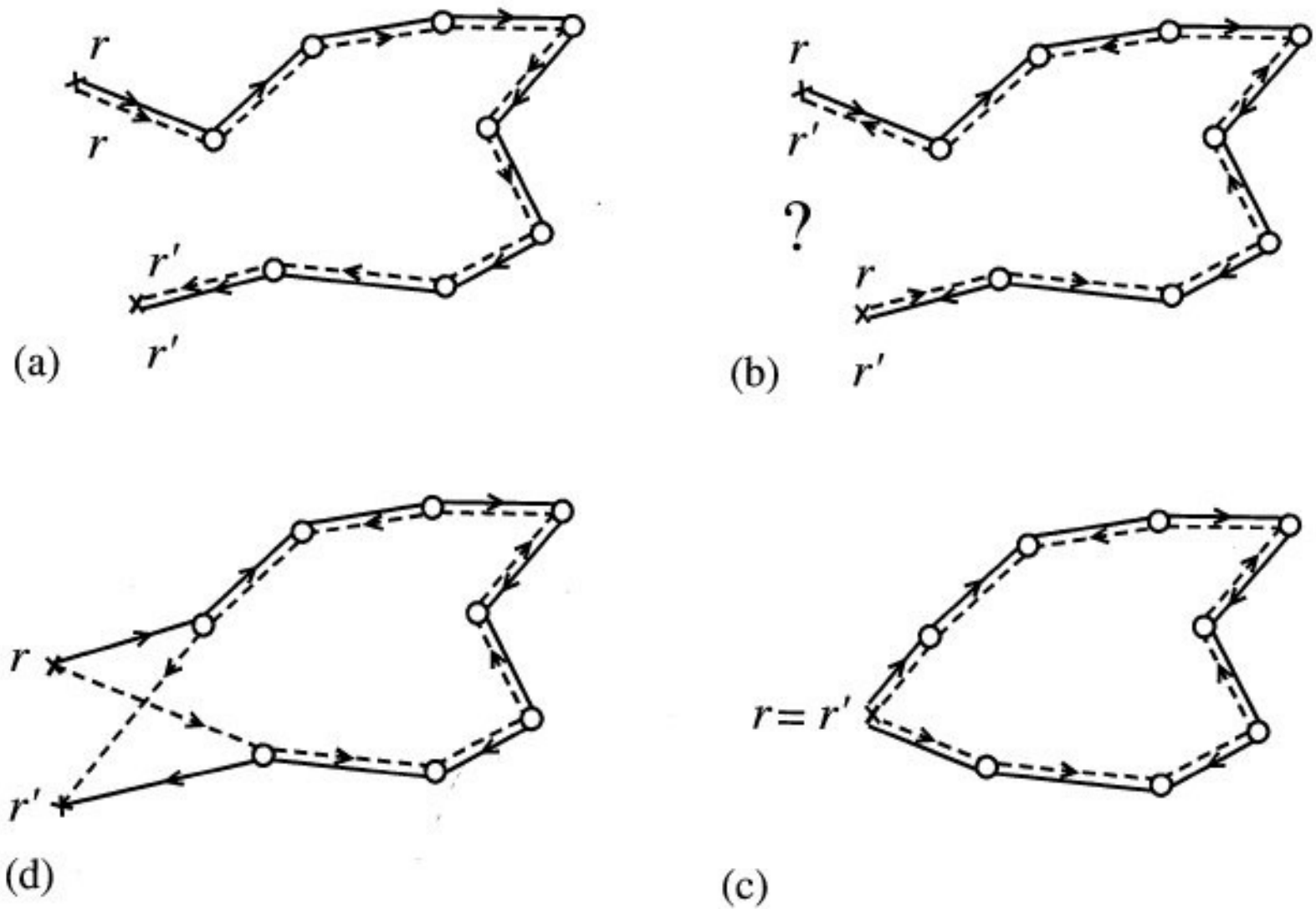

Figure 4.7 (a) Diffuson contribution to the probability. (b) Reversing one of the two trajectories, the points $\boldsymbol{r}$ and $\boldsymbol{r}'$ are exchanged, leading to an impossibility unlike $\boldsymbol{r}$ and $\boldsymbol{r}'$ coincide. In such a case (c), the phases cancel in this new contribution. (d) If $\boldsymbol{r} \neq \boldsymbol{r}'$, there is a mismatch between the two trajectories, leading to a phase shift.

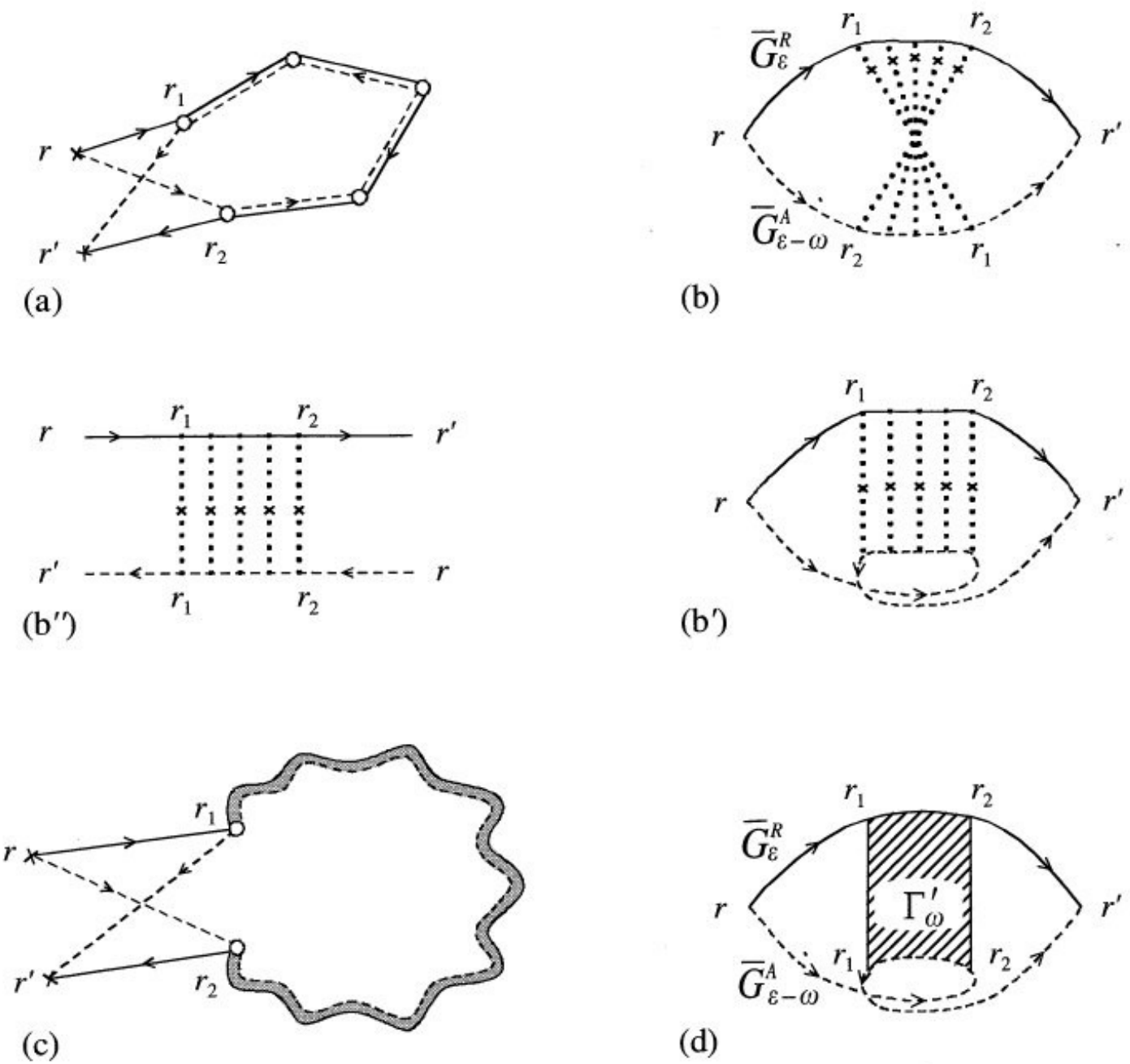

Figure 4.8 (a, b, b′, b″) Several equivalent representations of a process of five collisions which contribute to X_c. Representation (b) is common in the literature, and is called a Cooperon or *maximally crossed diagram*. Reversing one of the two trajectories (b → b′ → b″), we see that the Cooperon has a ladder structure very similar to that of the Diffuson. (c,d) Representations of X_c. These two figures should be compared with Figures 4.4(c,d) and demonstrate why the Cooperon is a short range

One out of many experimental studies of weak localization

VOLUME 54, NUMBER 14 PHYSICAL REVIEW LETTERS 8 APRIL 1985

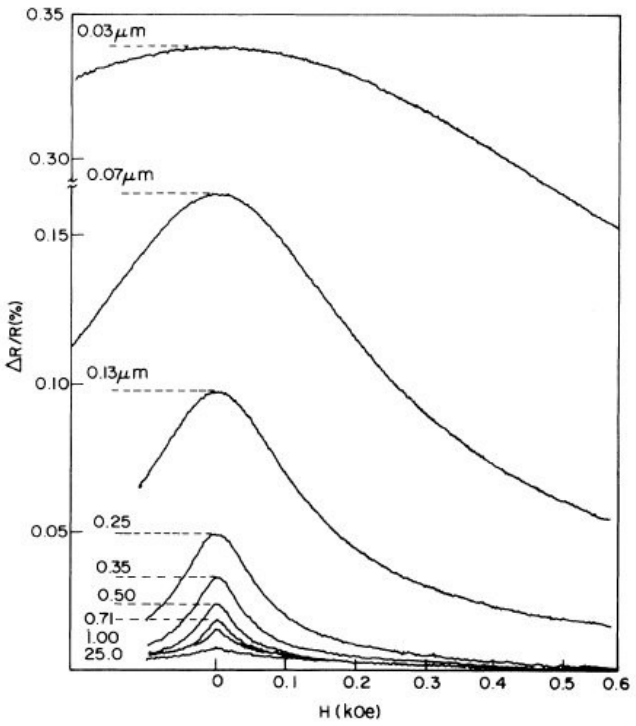

FIG. 1. Magnetoresistance data for L_i films varying in width, W, down to 0.03 ± 0.01 μm.

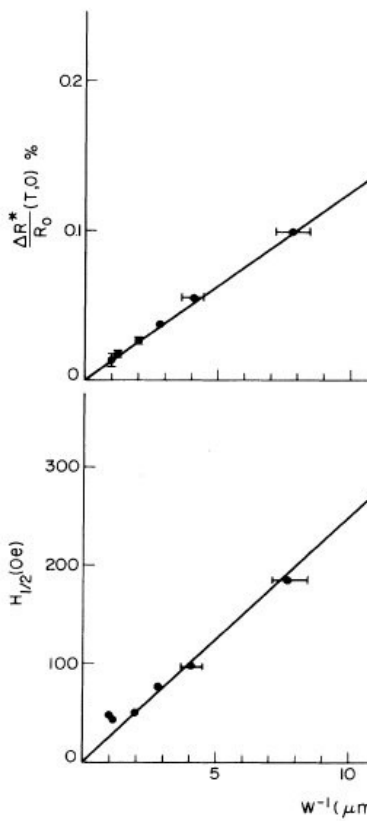

FIG. 2. The magnetoresistance peak height $\Delta R/R$ and peak width $H_{1/2}$ for the data of Fig. 1, vs W^{-1}.

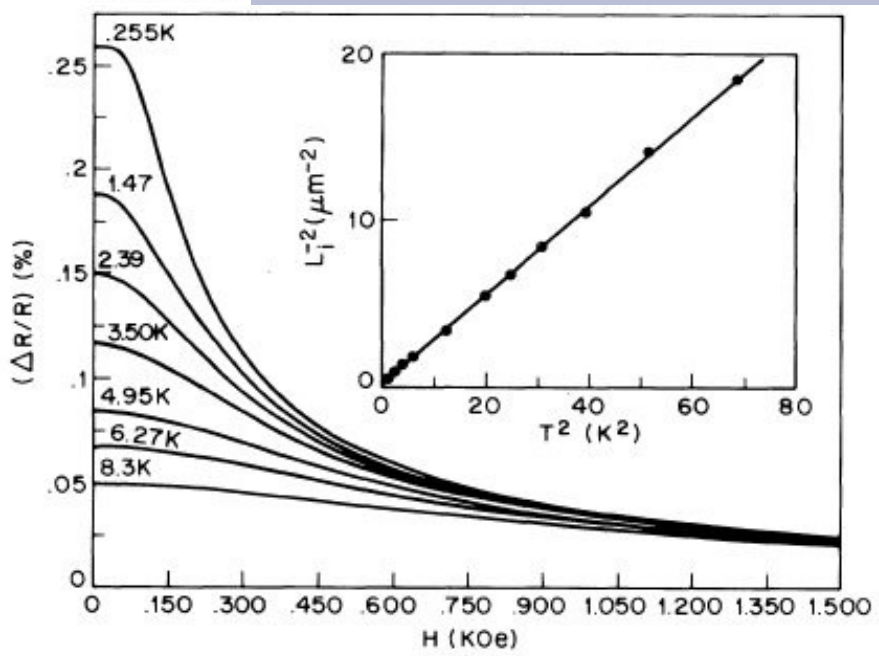

FIG. 3. Detailed fits of magnetoresistance data at various temperatures for $W = 0.074$ μm. Except for the elimination of noise, the fitted curves are indistinguishable from the data. Inset: Values for the quantity $\tilde{L}_i(T)^{-2}$ as a function of T^2 for part of our temperature range.

Two-dimensional quasi 1D normal metal strips of width W
Licini, Dolan, Bishop (1985)

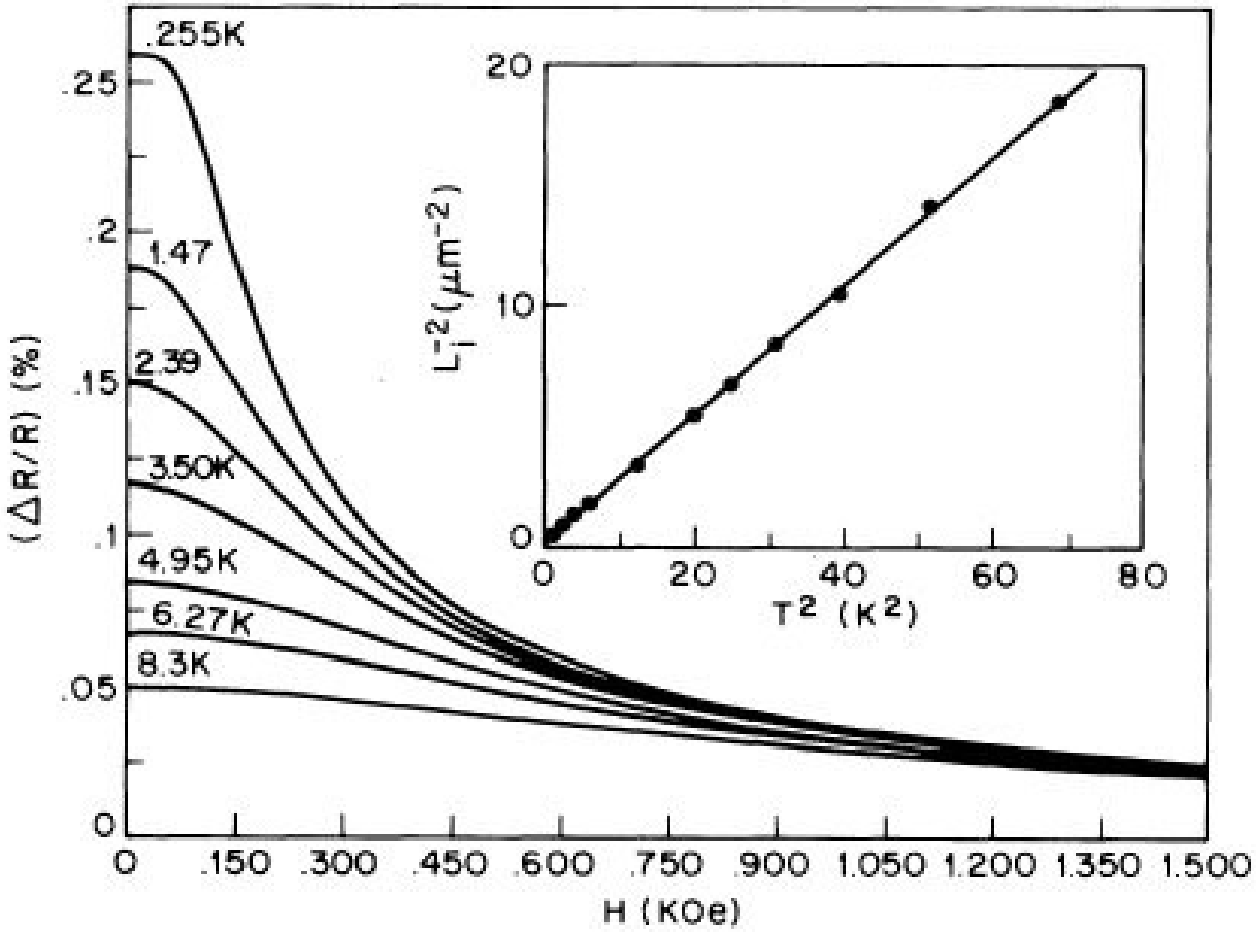

FIG. 3. Detailed fits of magnetoresistance data at various temperatures for $W = 0.074\ \mu$m. Except for the elimination of noise, the fitted curves are indistinguishable from the data. Inset: Values for the quantity $\tilde{L}_i(T)^{-2}$ as a function of T^2 for part of our temperature range.

This page was intentionally left blank

Aharonov-Bohm effect in conductors

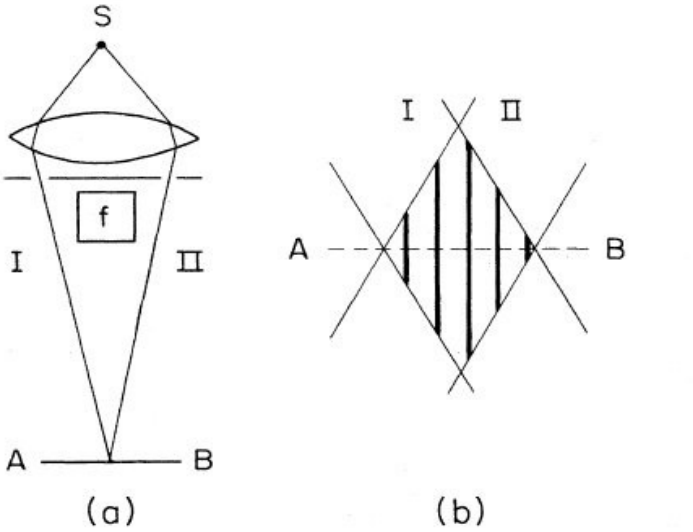

FIG. 1. (a) Schematic of electron-beam interference experiment (Ehrenberg and Siday, 1949); (b) the stationary wave pattern in the beam crossing region of space near the plane *AB*.

$$\Delta\varphi = \frac{e}{\hbar c}\oint \mathbf{A}\,dl = 2\pi\frac{\phi}{\phi_0}, \qquad \phi_0 = hc/e = 4.14\times10^{-7}\ \mathrm{G\,cm^2}$$

$$E_n = \frac{\hbar^2}{2mR^2}\left[n-\frac{\phi}{\phi_0}\right]^2, \qquad M = \frac{e\hbar}{2mc}\left[n-\frac{\phi}{\phi_0}\right].$$

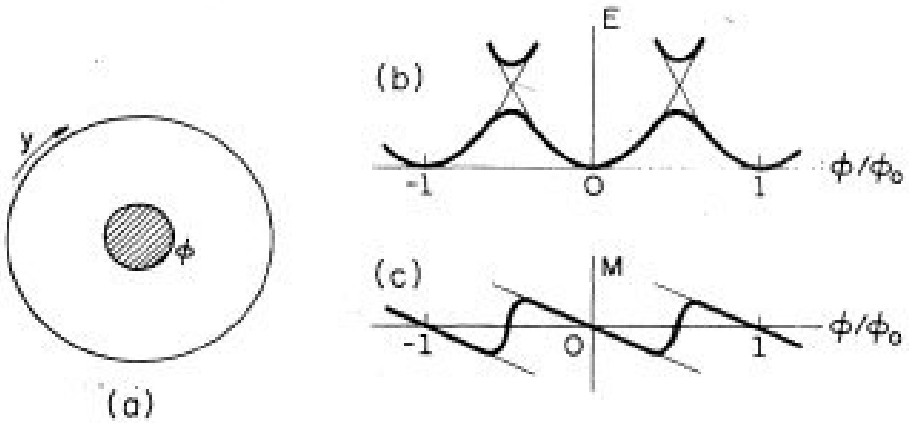

FIG. 2. (a) Schematic of one-dimensional ring confining a magnetic flux; (b) electron energy in the ring reduced magnetic flux ϕ/ϕ_0; (c) magnetic moment vs reduced flux ϕ/ϕ_0.

A within the sample should be nonzero, its tangential component being equal to $\phi/2\pi R$ (the Aharonov-Bohm experiment geometry). We assume that the mean free

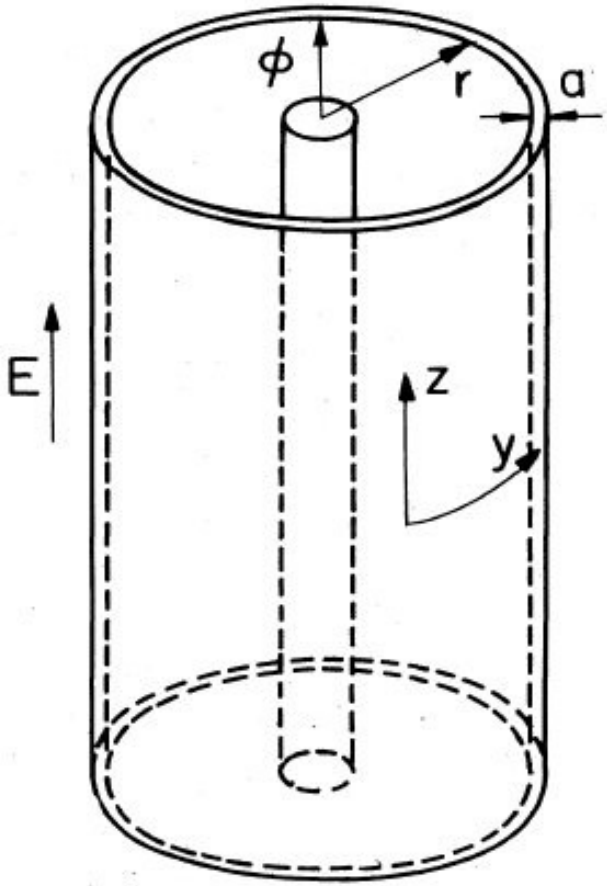

FIG. 5. Schematic of experiment with a solenoid carrying magnetic flux ϕ inside a cylinder with wall thickness a.

In the presence of the vector potential **A** of magnetic field, the equation for the cooperon takes on the form (Altshuler, Khmelnitskii, Larkin, and Lee, 1980)

$$\hbar\left[D\left[-i\nabla-\frac{2e}{c}\mathbf{A}\right]^2+i\omega+\frac{1}{\tau_\varphi}\right]C_\omega(\mathbf{r},\mathbf{r}')=\delta(\mathbf{r}-\mathbf{r}')\ . \tag{2.9}$$

Equation (2.9) resembles the Schrödinger equation for a particle of charge $2e$ and mass $\hbar/2D$ with the imaginary energy $i\omega$.

For a thin-walled hollow cylinder with magnetic field in the walls $H=0$ and vector potential $\mathbf{A}\neq 0$, constant in absolute magnitude and directed tangentially, the solution of Eq. (2.9) with periodic boundary conditions along the coordinate y (i.e., along the cylinder circumference), has the form

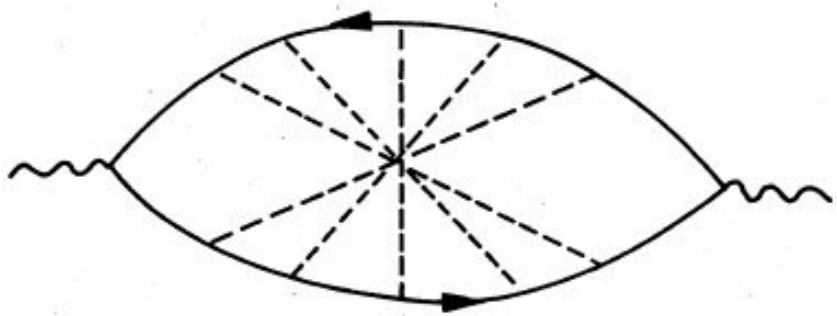

FIG. 6. Fan diagram for the conjugated wave interference.

AB-effect with a double-flux quantum period $\Phi_0=2hc/e$

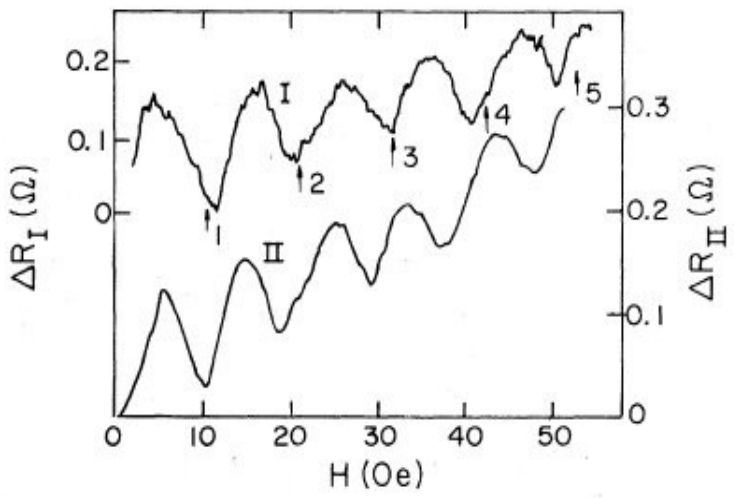

FIG. 7. Longitudinal magnetoresistance $\Delta R(H)$ at $T=1.1$ K for two cylindrical magnesium films on quartz filaments 1 cm long. $R_{4.2I}=9.2$ kΩ, $R_{4.2II}=12.3$ kΩ. The ratios $R_{300}/R_{4.2}$ for the two films are 1.39 and 1.25, respectively. Filament diameter of sample I measured with scanning electron microscope is 1.59 ± 0.03 μm. The arrows specify the fields corresponding to integer numbers of magnetic flux quanta $\phi_0/2=hc/2e$ through the filament cross-section area (Sharvin and Sharvin, 1981).

10 Oe = 1 mT

$C_\omega(\mathbf{r},\mathbf{r}')$ or "cooperon." The conductivity correction is related to the cooperon by the expression

$$\frac{\Delta\sigma(\omega)}{\sigma}=-\frac{2}{\pi\nu}C_\omega(\mathbf{r},\mathbf{r}) , \tag{2.8}$$

where ν is the density of states at the Fermi level and σ is connected with the diffusion coefficient through Einstein's relation

$$\sigma=e^2D\nu .$$

In the presence of the vector potential $\mathbf{A}$ of magnetic field, the equation for the cooperon takes on the form (Altshuler, Khmelnitskii, Larkin, and Lee, 1980)

$$\hbar\left[D\left[-i\nabla-\frac{2e}{c}\mathbf{A}\right]^2+i\omega+\frac{1}{\tau_\varphi}\right]C_\omega(\mathbf{r},\mathbf{r}')=\delta(\mathbf{r}-\mathbf{r}') . \tag{2.9}$$

Equation (2.9) resembles the Schrödinger equation for a particle of charge $2e$ and mass $\hbar/2D$ with the imaginary energy $i\omega$.

$$C_\omega(\mathbf{r},\mathbf{r}')=\frac{1}{2\pi\hbar R}\int\frac{d\mathbf{Q}_\perp}{(2\pi)^2}\sum_{l=-\infty}^{\infty}e^{i\mathbf{Q}(\mathbf{r}-\mathbf{r}')}\frac{1}{i\omega+\frac{1}{\tau_\varphi}+DQ_\perp^2+D\left[Q_y^l-\frac{2e}{c}A\right]^2}, \tag{2.10}$$

where $\mathbf{Q}_\perp=(Q_x,Q_z)$, $Q_y^l=l/R$, and R is the cylinder radius. Substituting Eq. (2.10) in Eq. (2.8) yields

$$\Delta\sigma(\omega)=-\frac{2e^2}{\pi\hbar}\frac{1}{2\pi R}\int\frac{d\mathbf{Q}_\perp}{(2\pi)^2}\sum_{l=-\infty}^{\infty}\frac{1}{Q_\perp^2+L_\varphi^{-2}(\omega)+\frac{1}{R^2}\left[n-\frac{2\phi}{\phi_0}\right]^2}, \qquad L_\varphi^2(\omega)=\frac{L_\varphi^2}{1+i\omega\tau_\varphi} \tag{2.11}$$

If the thickness of the cylinder walls is small compared with the length $L_\varphi(\omega)$, then the integration over Q_x should be replaced by a summation with only the term corresponding to $Q_x=0$ retained. If, in addition, the cylinder height is also small compared with $L_\varphi(\omega)$, then the integral over Q_z should be likewise replaced by a sum, with only the term with $Q_z=0$ retained in it (thin ring). This yields for the conductance of a unit length along the circumference of a thin ring $G_1=\sigma ab$ (b is the ring height, a is the ring thickness)

$$\Delta G_1(\omega)=-\frac{e^2}{\pi\hbar}L_\varphi(\omega)\times\sum_{l=-\infty}^{+\infty}\frac{1}{\pi}\frac{R/L_\varphi(\omega)}{\left[\frac{R}{L_\varphi(\omega)}\right]^2+\left[l-\frac{2\phi}{\phi_0}\right]^2}. \tag{2.12}$$

For $\omega=0$, Eq. (2.12) can be presented in the form (Altshuler, Aronov, and Spivak, 1981)

$$\Delta G_1=-\frac{e^2L_\varphi}{\pi\hbar}\frac{\sinh\frac{2\pi R}{L_\varphi}}{\cosh\frac{2\pi R}{L_\varphi}-\cos 2\pi\frac{2\phi}{\phi_0}}. \tag{2.13}$$

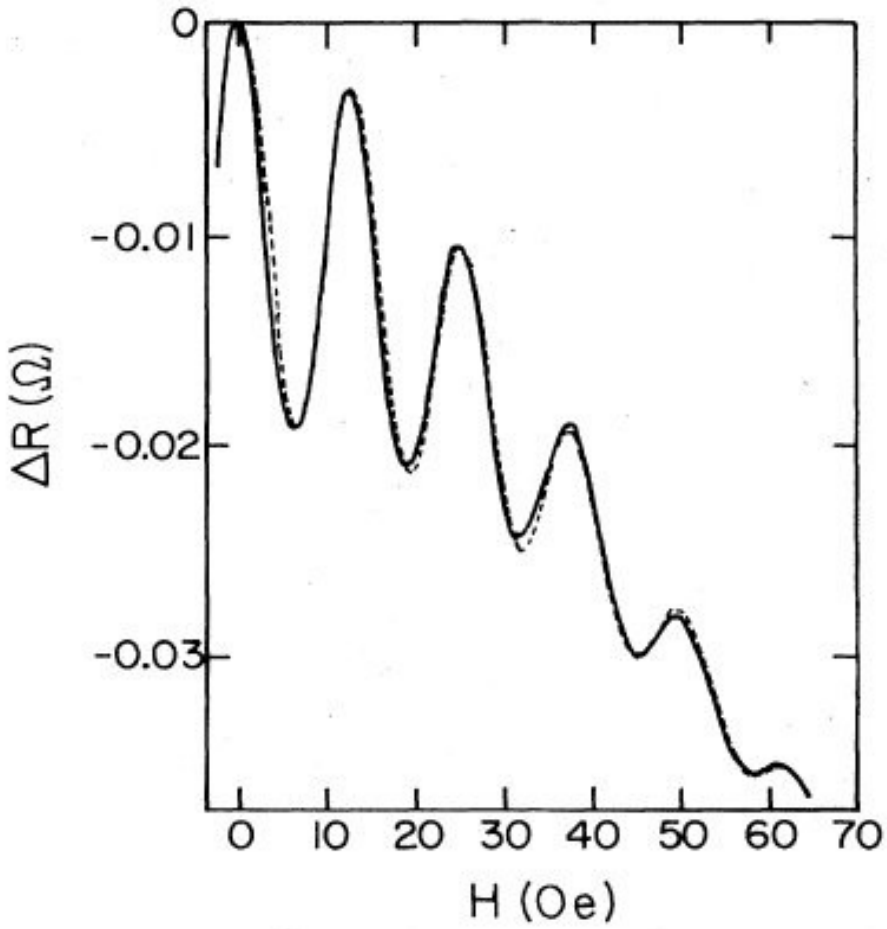

FIG. 8. Longitudinal magnetoresistance $\Delta R(H)$ at $T=1.1$ K for a cylindrical lithium film evaporated onto a 1-cm-long quartz filament. $R_{4.2}=2$ kΩ, $R_{300}/R_{4.2}=2.8$. Solid line: averaged from four experimental curves. Dashed line: calculated for $L_\varphi=2.2$ μm, $\tau_\varphi/\tau_{so}=0$, filament diameter $d=1.31$ μm, film thickness 127 nm. Filament diameter measured with scanning electron microscope yields $d=1.30\pm0.03$ μm (Altshuler *et al.*, 1982; Sharvin, 1984).

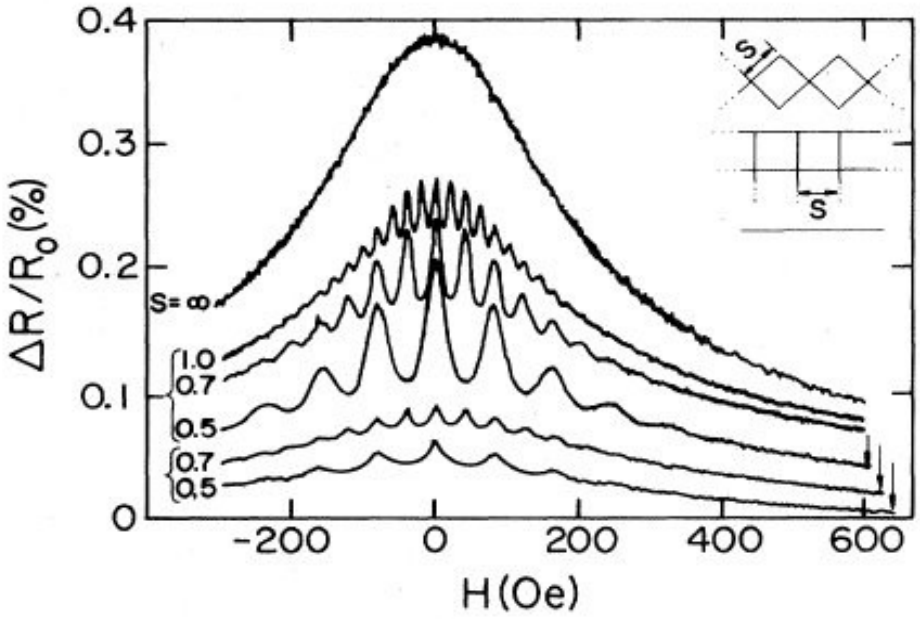

FIG. 12. Transverse magnetoresistance $R(H)$ for $T=0.13$ K for lithium strips 21 ± 1 nm thick and 55 ± 7 nm wide. Uppermost curve, wire control sample; next three curves, three necklace arrays; bottom two curves, two meshes. Some of the curves have been displaced vertically for clarity. The size S in μm of the unit cell side is indicated next to each curve. The upper right-hand sketches define the necklace, mesh, and control geometries, respectively. Measurements of $R(H,T)$ on the control sample yielded values for the diffusion L_φ of $(1.85\pm0.1)\times T^{-1}$ μm, $L_{so}=2.3\pm0.2$ μm, $L_s=3.1\pm0.2$ μm (Dolan *et al.*, 1985).

Mesoscopic AB-effect with a single-quantum period $\Phi_0=hc/e$

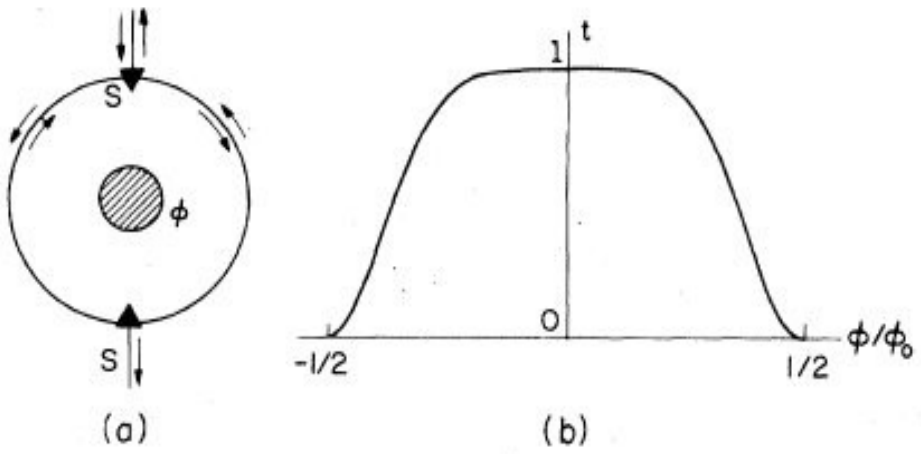

FIG. 3. (a) Schematic of one-dimensional ring with scatterers S and current-carrying contacts by Büttiker *et al.* (1984); (b) relative transmitted wave intensity vs reduced magnetic flux ϕ/ϕ_0.

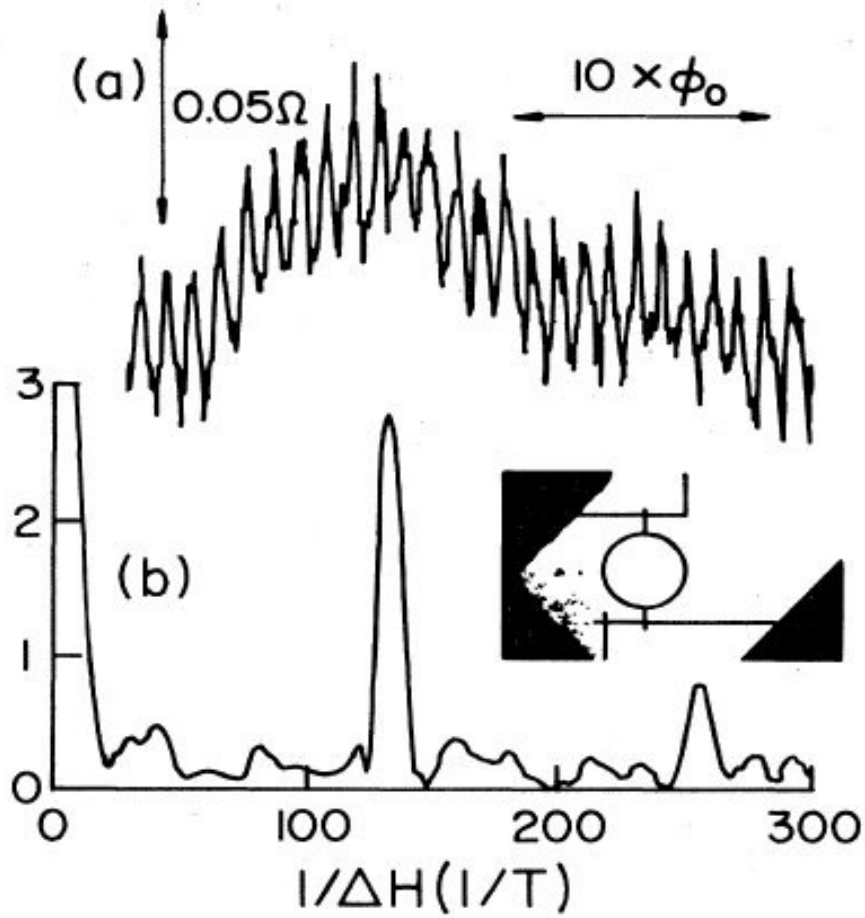

FIG. 17. (a) Gold ring magnetoresistance at 0.01 K (Webb *et al.*, 1985). (b) Fourier power spectrum in arbitrary units. Inset: picture of the ring.

Magnetoresistance in a larger field range: coexistence of AB effect and mesoscopic fluctuations

- Mesoscopic sample-specific fluctuations sampled by conductance dependence on some parameter (e.g. gate voltage, E or B fields)
- Typical conductance variation e^2/h
- The period of AB effect is single-flux quantum (lack of avreraging)

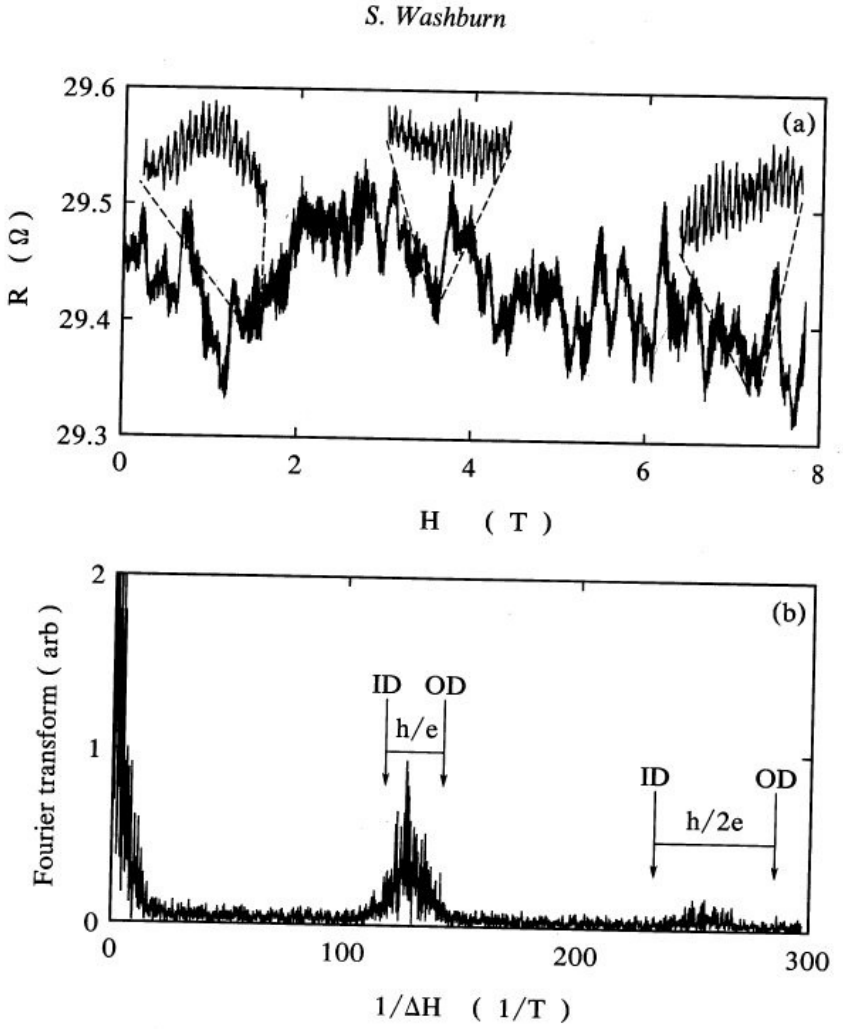

Fig. 6. (a) The magnetoresistance of the loop from fig. 5 over a wider range of magnetic field. The insets depict the periodic oscillations that pervade the entire field range. (b) The Fourier transform of the data in (a). The arrows mark the magnetic field frequencies for flux h/e and $h/2e$ through the areas enclosed by the inside and outside perimeters of the loop.

Averaging over many rings

Umbach et al. PRL 56, 386 (1986)

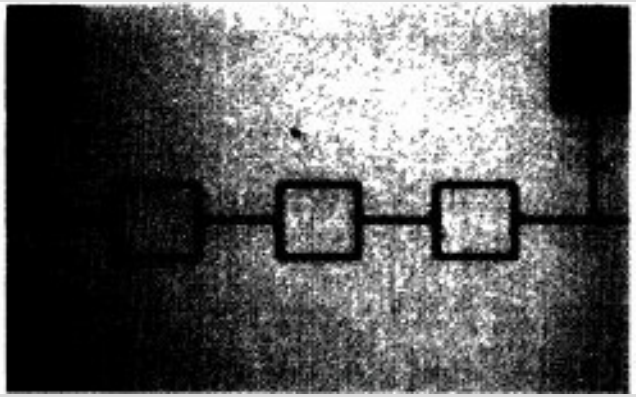

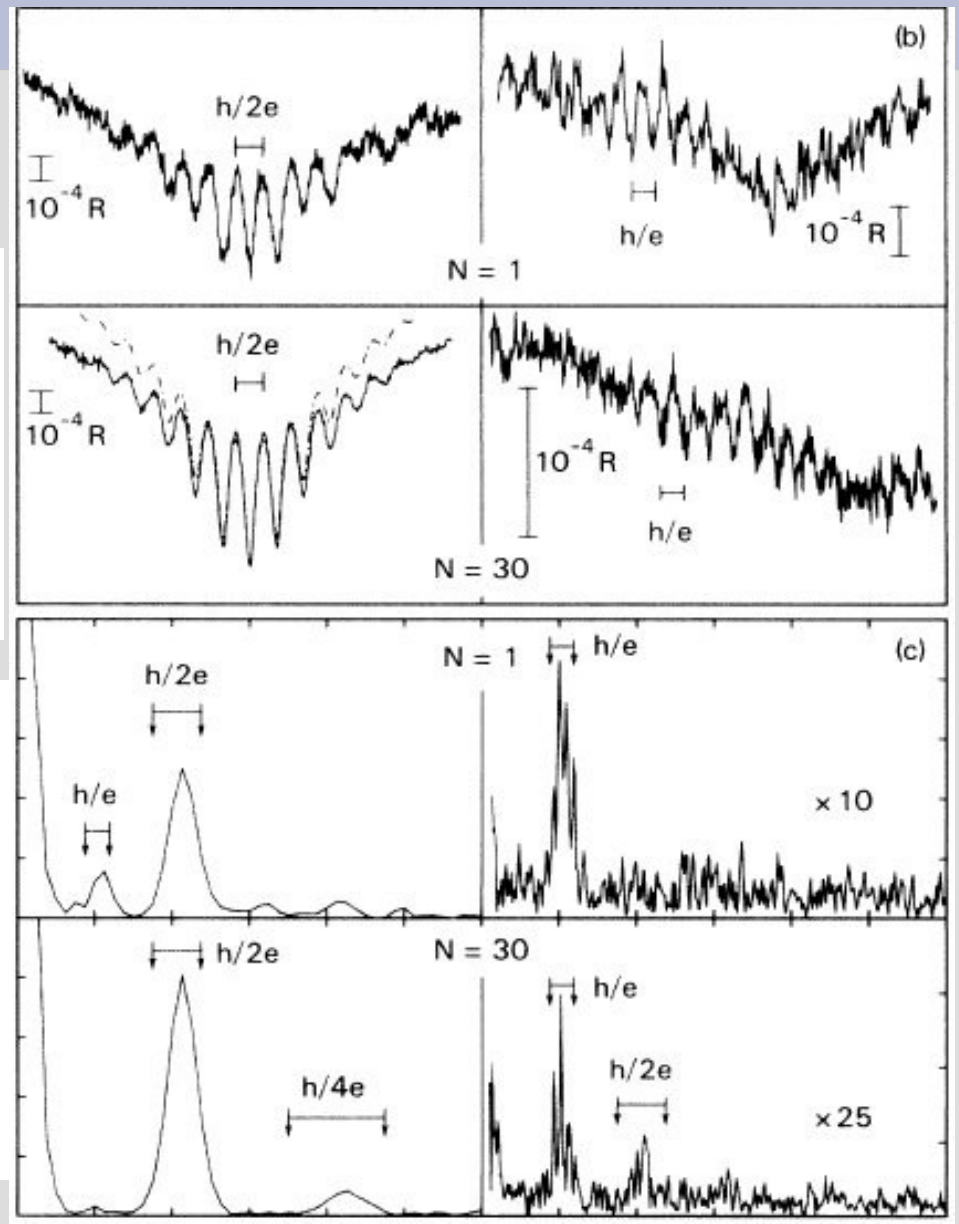

FIG. 1. (a) Transmission electron micrograph of the three-loop sample. (b) Magnetoresistance data at $T = 0.32$ K. Clockwise from the lower right-hand corner: the thirty-loop sample for $0.2 < H < 0.3$ T; the thirty-loop sample for $-0.02 < H < 0.02$ T (the dash-dotted line is the fit by the AAS theory); the single-loop sample for $-0.02 < H < 0.02$ T; the single-loop sample for $0.15 < H < 0.25$ T. (c) The Fourier transforms of the data in (b). The arrows in the figure indicate the bounds for the flux periods h/e and $h/2e$ based on the measured inside and outside areas of the loop.

Univerasal conductance fluctuations

Boris Altshuler, Patrick Lee, Doug Stone simulatneously (1985)

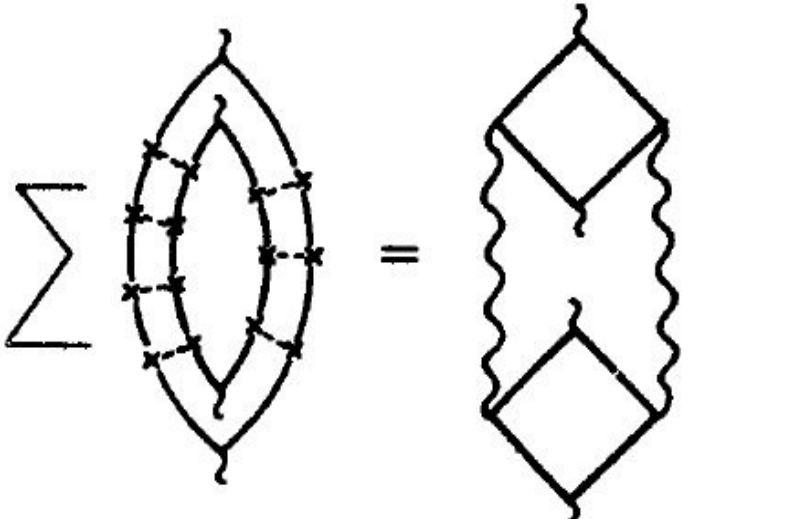

B. L. Al'tshuler

JETP Lett., Vol. 41, No. 12, 25 June 1985

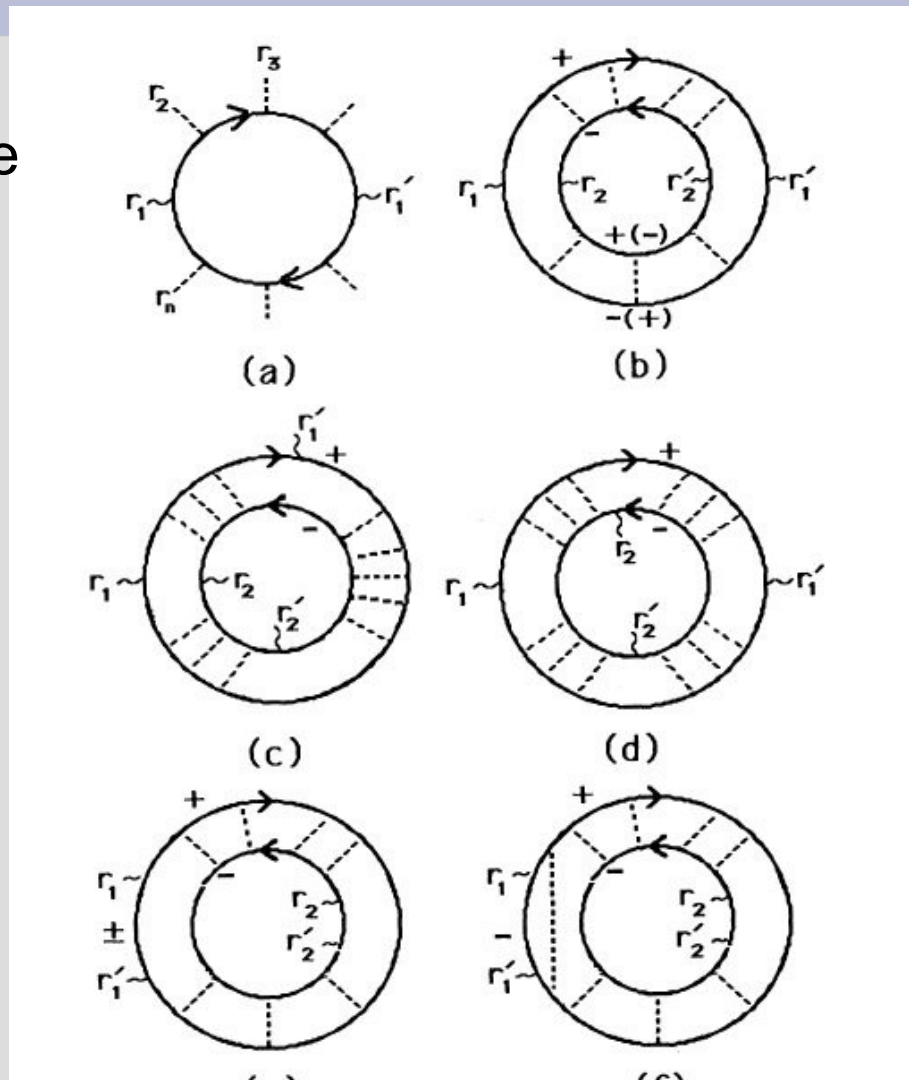

FIG. 1. (a) Unaveraged conductance. (b)–(f) Diagrams contributing to the correlation function; (e) and (f) are examples of a class of diagrams which cancel each other.

Antilocalization in the presence of spin-orbital scattering

- Sign reversal of weak localization (Hikami, Larkin, Nagaoka, Prog. Theor. Phys. 63, 707 (1980))
- Pancharatnam-Berry phase argument, generalized for random scattering (Meir, Gefen, Entin-Wohlmann, PRL 63, 798 (1989))
- Measured directly via AB oscillation period splititng (Morpurgo et al. PRL80, 1050 (1998))

Anandan, Christian and Wanelik "Geometric phases in physics". Am. J. Phys. 65: 180 (1997).

problem). SO interaction modifies the ϕ dependence of the bare-problem spectrum into a $\phi \pm \delta$ dependence, for the two relevant spin directions. Here δ characterizes the SO scattering in the sample. Consequently, any thermodynamic or transport property of the system, $Q(\phi)$, which does not depend explicitly on spin (more precisely, does not involve operators that mix the two spin orientations) can be expressed in the form

$$Q(\phi) = \tfrac{1}{2}\,[Q_0(\phi+\delta)+Q_0(\phi-\delta)]\,,$$

where Q_0 is the corresponding bare system quantity.

We find that, *upon averaging*, all odd harmonics vanish; the $n=2$ harmonic is multiplied by $-\frac{1}{2}$, the $n=4$ by $\frac{1}{8}$, etc. The magnitude of the fluctuations of the $n=1$ harmonic is reduced, *upon averaging*, by a factor of $\frac{1}{4}$, that of the $n=3$ by $\frac{7}{16}$, and so on. Somewhat more compli-

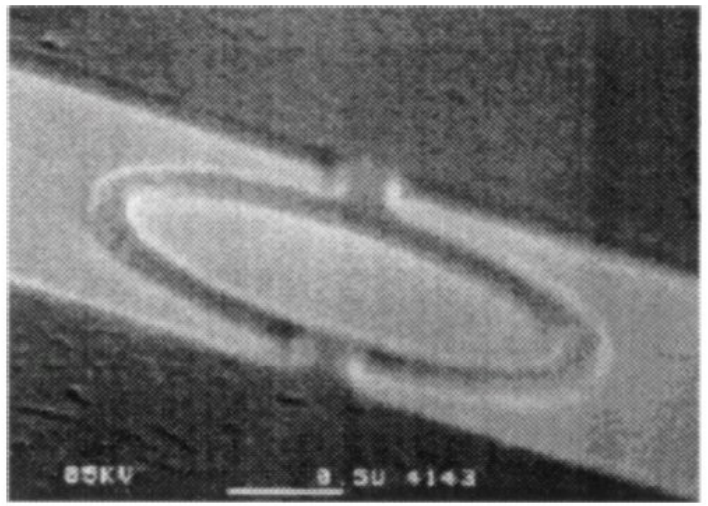

FIG. 1. One of the rings used in our investigations. The white bar shown is 0.5 μm long.

Berry phase in SO scattering

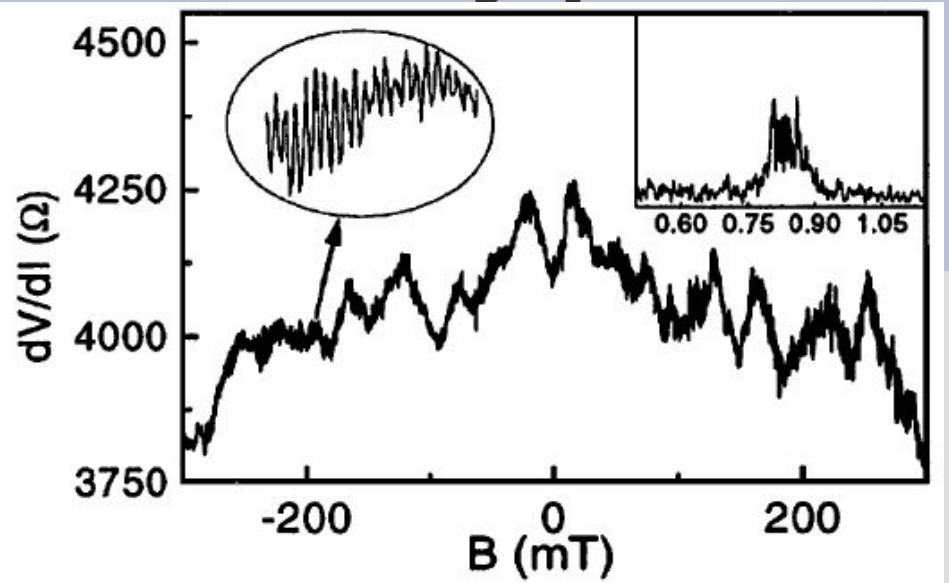

FIG. 2. Single magnetoresistance trace measured in the AB ring discussed in the text. The insets show an enlargement of the conductance oscillations and the peak in their Fourier spectrum (x axis units are in mT^{-1}).

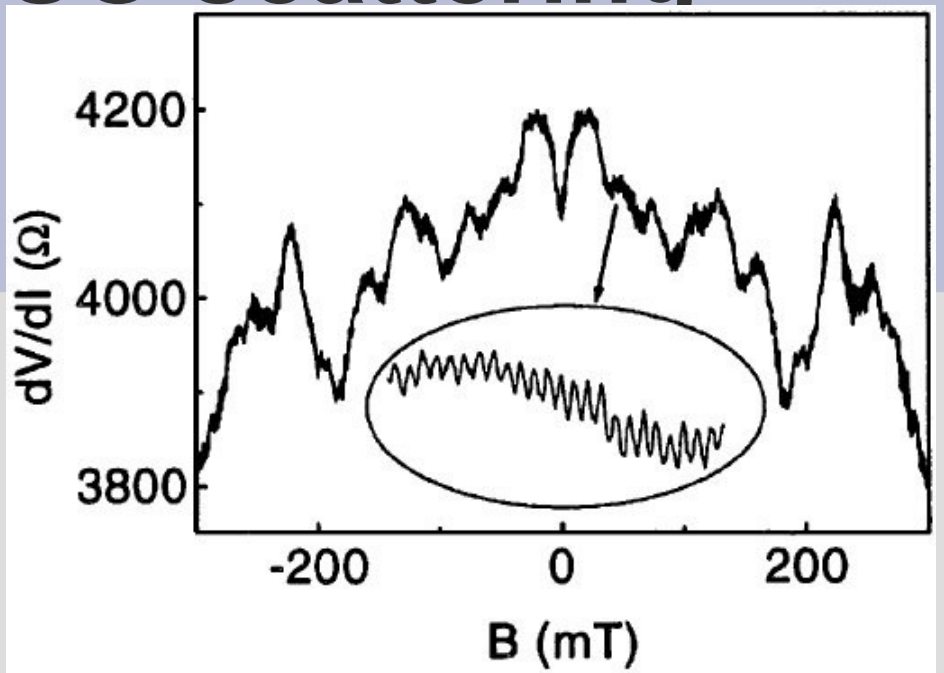

FIG. 3. Average of $\simeq 30R(B)$ curves (the inset is an enlargement of the small part of the curve). Note how the reciprocity relation is rather accurately satisfied, far better than in the data

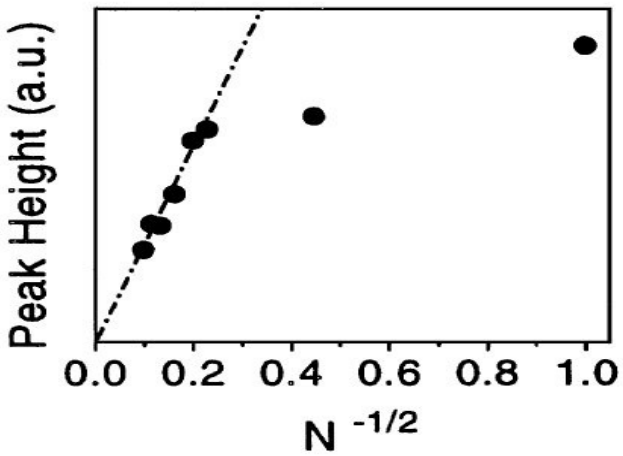

FIG. 4. Height of the peak in the Fourier spectrum of the average $R(B)$ curve as a function of the inverse square root of the number of traces involved in the average. The line shows that for sufficiently large N the height decays linearly with $N^{-1/2}$ and extrapolates to 0, as expected for an ensemble average. For small N this is not true because consecutively measured $R(B)$ traces are not completely uncorrelated.

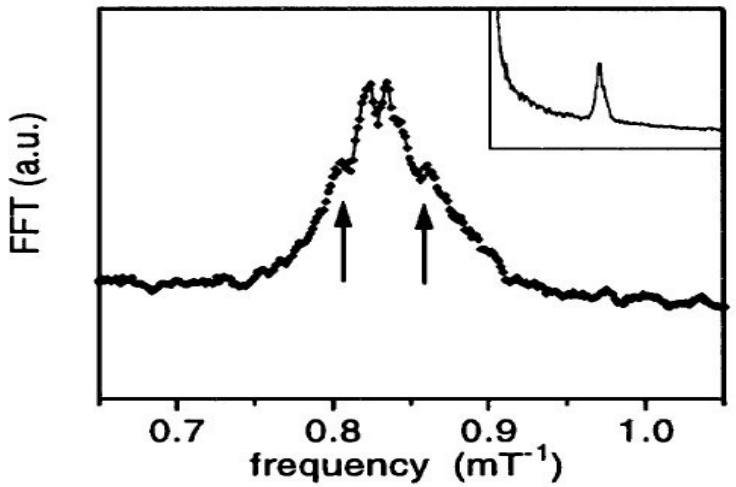

FIG. 5. The peak of the average Fourier spectrum: the splitting is evident, as well as some structure on the sides (pointed by the arrows). The inset shows the same curve on a larger frequency range: note the presence of $1/f$ noise resulting from the switching events.

?

Anderson localization Anderson (1957)

A non-interacting electron in a random potential may be localized.

Gang of four (1979): scaling theory

Weak localization P.A. Lee, H. Fukuyama, A. Larkin, S. Hikami, ….

well-understood area in condensed-matter physics

Unsolved problems:

Theoretical description of critical points

Scaling theory for critical phenomena in disordered systems

A non-interacting electron moving in random potential

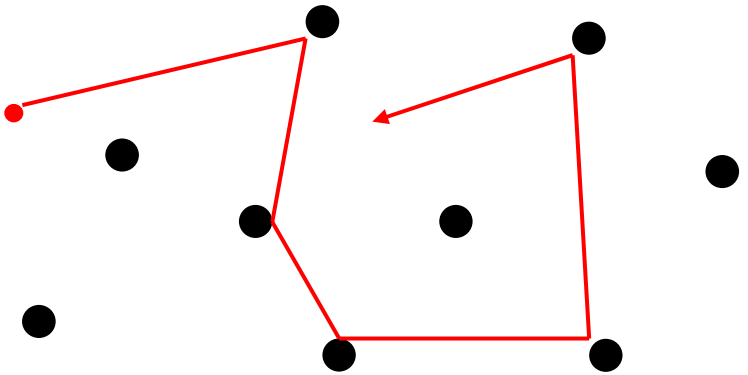

Quantum interference of scattering waves

⇒ Anderson localization of electrons

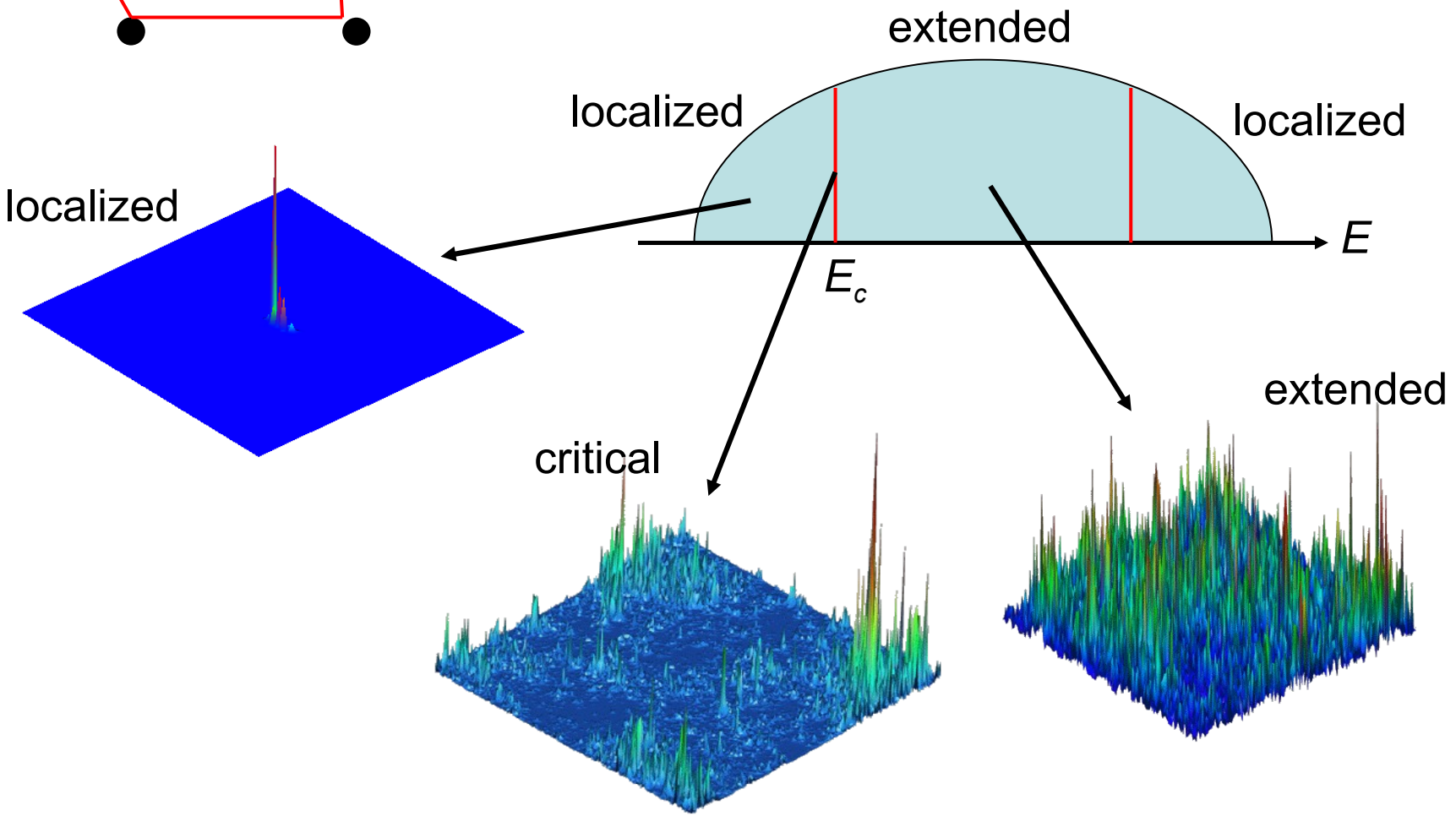

Scaling theory (gang of four, 1979)

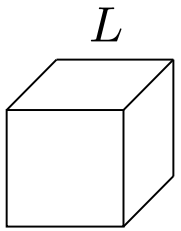

Conductance g changes when system size is L changed

Metal: $g \propto \dfrac{\text{area}}{\text{length}} = L^{d-2}$

Insulator: $g \propto e^{-L/\xi}$

$$\beta(g) = \frac{d \ln g}{d \ln L} = d - 2 - \mathcal{O}(g^{-1})$$

$$g \gg 1$$

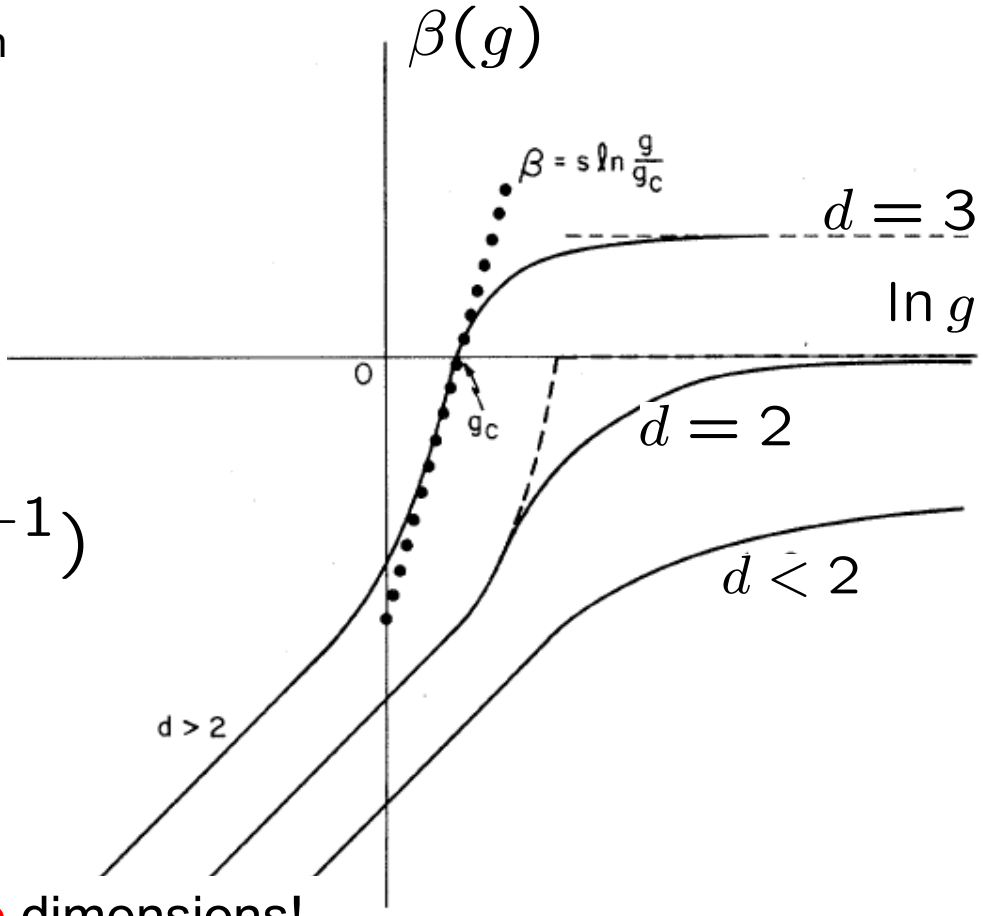

All wave functions are localized below two dimensions!

A metal-insulator transition at $g=g_c$ is continuous (d>2).

Prog. Theor. Phys. Vol. 63, No. 2, February 1980, Progress Letters

Spin-Orbit Interaction and Magnetoresistance in the Two Dimensional Random System

Shinobu HIKAMI, Anatoly I. LARKIN*) and Yosuke NAGAOKA
Research Institute for Fundamental Physics
Kyoto University, Kyoto 606

(Received November 5, 1979)

3 symmetry classes (orthogonal, unitary, symplectic)

symplectic class: ○ time-reversal, × spin-rotation
spin-orbit interaction

anti-localization

$$\frac{d\ln g}{d\ln L} = d - 2 + \frac{c}{g} \qquad c > 0$$

Metal-insulator transition in 2D

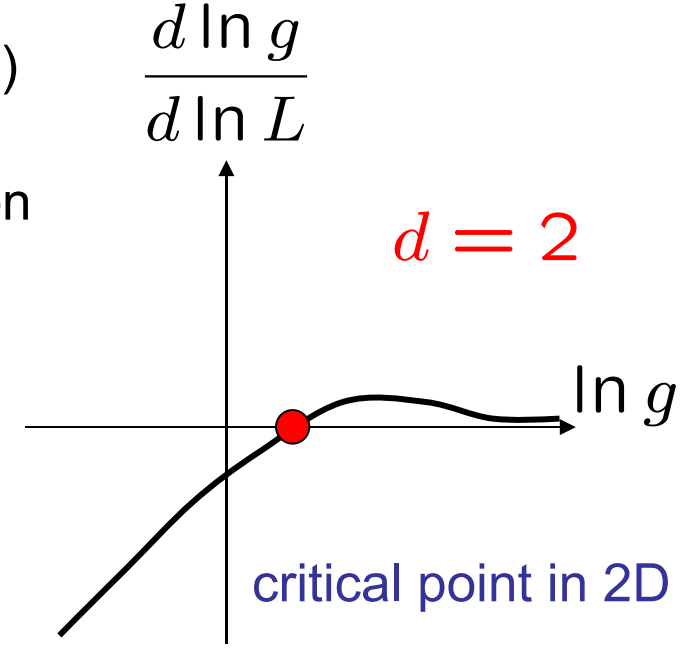

?

PHYSICAL REVIEW VOLUME 109, NUMBER 5 MARCH 1, 1958

Absence of Diffusion in Certain Random Lattices

P. W. ANDERSON
Bell Telephone Laboratories, Murray Hill, New Jersey

4202 citations!

What if I place a particle in a random potential and wait?

Tight binding model

$$\epsilon_i a_i^\alpha - \sum_j V_{ij} a_j^\alpha = E^\alpha a_i^\alpha.$$

V_{ij} nearest neighbors, ε_i random potential

Technique: Looking for inestabilities in a locator expansion

Not rigorous! Small denominators

Correctly predicts a metal-insulator transition in 3d and localization in 1d

Interactions?

Disbelief?, against the spirit of band theory

But my recollection is that, on the whole, the attitude was one of humoring me.

A selfconsistent theory of localization

J. Phys. C Vol. 6, 1973 1734

R Abou-Chacra†, P W Anderson‡§ and D J Thouless†

Perturbation theory around the insulator limit (locator expansion).

$$\epsilon_i a_i^\alpha - \sum_j V_{ij} a_j^\alpha = E^\alpha a_i^\alpha .$$

$$E - \epsilon_i - S_i(E) = \{G_{ii}(E)\}^{-1}$$

$$S_i(E) = \sum_{j \neq i} \frac{|V_{ij}|^2}{E - \epsilon_j - S_j(E)}$$

No control on the approximation.

It should be a good approx for d>>2.

It predicts correctly localization in 1d and a transition in 3d

The distribution of the self energy S_i (E) is sensitive to localization.

$$\Gamma = \mathrm{Im} S_i(E + i\eta)$$

$$\lim_{\eta \to 0} \lim_{V \to \infty} P(\Gamma) \begin{cases} > 0 & \text{metal} \\ = 0 & \text{insulator} \end{cases}$$

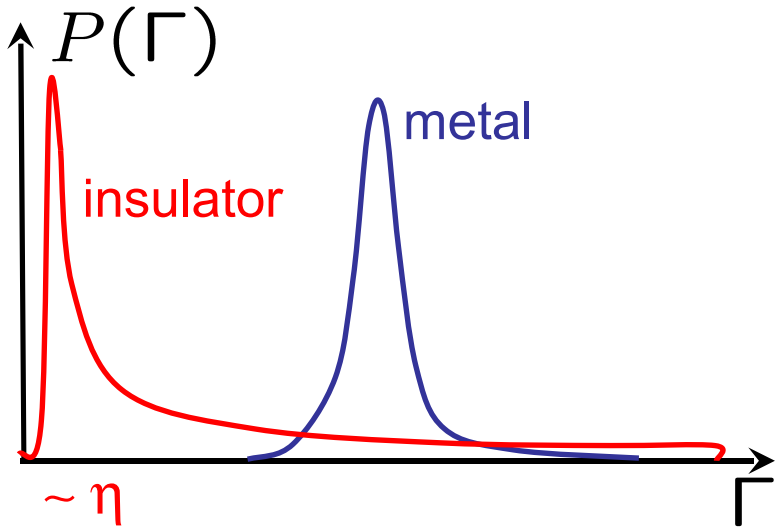

Scaling theory of localization

Phys. Rev. Lett. 42, 673 (1979), Gang of four. Based on Thouless,Wegner, scaling ideas

Energy Scales

1. Mean level spacing: $\delta = 1/\nu$
2. Thouless energy: $E_T = h / t_T$

$t_T(L)$ is the travel time to cross a box of size L

Dimensionless Thouless conductance

$$g \equiv \frac{E_T}{\delta}$$

Diffusive motion
without localization corrections

$$E_T = D\ L^{-2} \qquad \delta \propto L^{-d} \qquad g \propto L^{d-2}$$

$E_T >> \delta \quad g >> 1$ → **Metal**

$E_T << \delta \quad g << 1$ → **Insulator**

Scaling theory of localization

The change in the conductance with the system size only depends on the conductance itself

$\beta(g)$

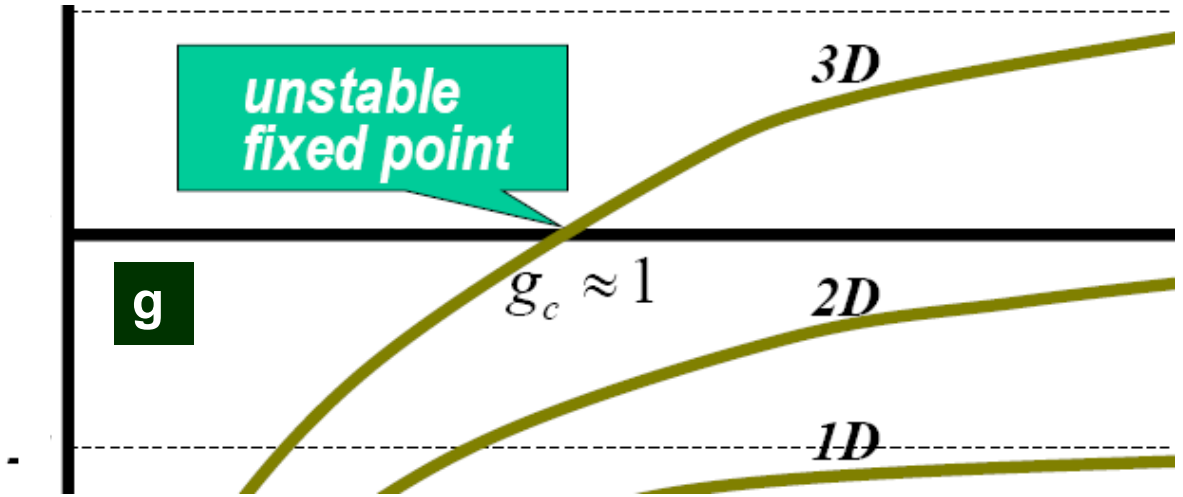

Weak localization

$$\frac{d \log g}{d \ln L} = \beta(g)$$

$g >> 1 \quad g \propto L^{d-2} \quad \beta(g) = (d-2) - \pi / g$

$g << 1 \quad g \propto e^{-L/\zeta} \quad \beta(g) \approx \log g < 0$

Predictions of the scaling theory at the transition

1. Diffusion becomes anomalous

$$\left\langle r^2(t) \right\rangle \propto t^{2/d}$$

2. Diffusion coefficient become size and momentum dependent

$$D(q) \propto q^{d-2} \qquad D(L) \propto L^{2-d}$$

Chalker

3. $g=g_c$ is scale invariant therefore level statistics are scale invariant as well

Weak localization

Positive correction to the resistivity of a metal at low T

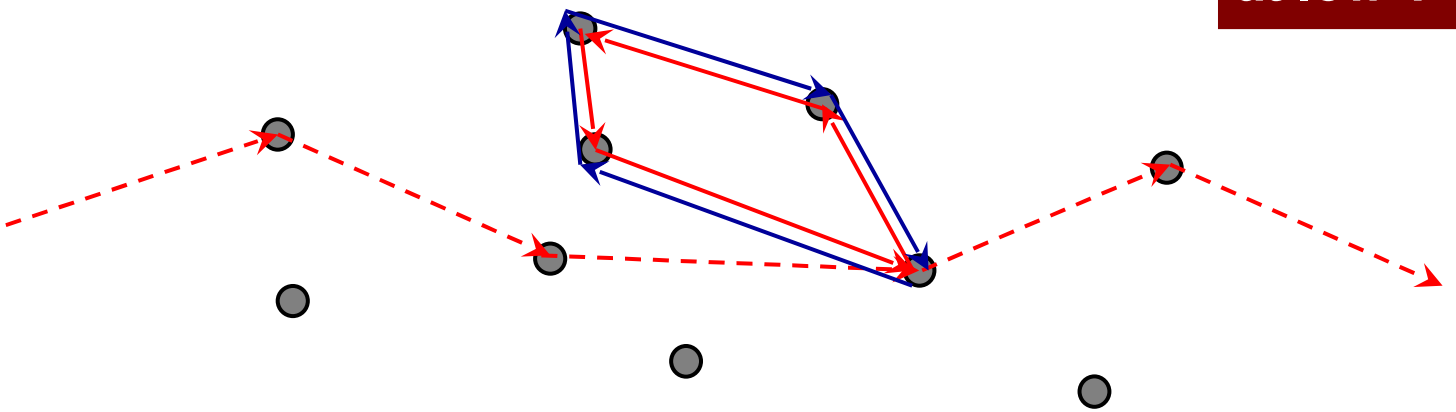

1.Cooperons (Langer-Neal, maximally crossed, responsible for weak localization) and Diffusons (no localization, semiclassical) can be combined.

3. Accurate in d ~2.

Self consistent condition (Wolfle-Volhardt)

$$D(\omega) = D_0 - \frac{k_F^{2-d}}{\pi m} \int_0^{k_0} dk \, \frac{k^{d-1}}{[-i\omega/D(\omega)] + k^2}$$

No control on the approximation!

Predictions of the self consistent theory at the transition

1. Critical exponents:

$$|\psi(r)| \quad e^{-r/\xi} \qquad \xi \propto |E - E_c|^{-\nu}$$

$$\nu = \frac{1}{d-2} \qquad d < 4$$

$$\nu = 1/2 \qquad d > 4$$

2. Transition for d>2

Disagreement with numerical simulations!!

3. Correct for d ~ 2

Why?

Why do self consistent methods fail for d = 3?

1. Always perturbative around the metallic (Vollhardt & Wolfle) or the insulator state (Anderson, Abou Chacra, Thouless) .

A new basis for localization is needed

2. Anomalous diffusion at the transition (predicted by the scaling theory) is not taken into account.

$$D(L) \propto L^{2-d}$$

$$D(q) \propto q^{d-2}$$